



Droplet-Based Microfluidics Reveals Insights into Cross-Coupling Mechanisms over Single-Atom Heterogeneous Catalysts

Journal Article

Author(s):

Moragues, Thomas ; Giannakakis, Georgios ; Ruiz-Ferrando, Andrea; Borca, Camelia N.; Huthwelker, Thomas; Bugaev, Aram; de Mello, Andrew J.; Pérez-Ramírez, Javier; Mitchell, Sharon

Publication date:

2024-05-13

Permanent link:

<https://doi.org/10.3929/ethz-b-000668061>

Rights / license:

[Creative Commons Attribution 4.0 International](#)

Originally published in:

Angewandte Chemie. International Edition 63(20), <https://doi.org/10.1002/anie.202401056>

Funding acknowledgement:

180544 - NCCR Catalysis (phase I) (SNF)

Heterogeneous Catalysis

Droplet-Based Microfluidics Reveals Insights into Cross-Coupling Mechanisms over Single-Atom Heterogeneous Catalysts

Thomas Moragues, Georgios Giannakakis, Andrea Ruiz-Ferrando, Camelia N. Borca, Thomas Huthwelker, Aram Bugaev, Andrew J. de Mello,* Javier Pérez-Ramírez,* and Sharon Mitchell*

Abstract: Single-atom heterogeneous catalysts (SACs) hold promise as sustainable alternatives to metal complexes in organic transformations. However, their working structure and dynamics remain poorly understood, hindering advances in their design. Exploiting the unique features of droplet-based microfluidics, we present the first *in-situ* assessment of a palladium SAC based on exfoliated carbon nitride in Suzuki–Miyaura cross-coupling using X-ray absorption spectroscopy. Our results confirm a surface-catalyzed mechanism, revealing the distinct electronic structure of active Pd centers compared to homogeneous systems, and providing insights into the stabilizing role of ligands and bases. This study establishes a valuable framework for advancing mechanistic understanding of organic syntheses catalyzed by SACs.

Cross-coupling reactions in fine chemical syntheses have long relied on organometallic metal complexes, which offer precise control over active site coordination spheres, resulting in exceptional activity and selectivity.^[1] However, their

soluble nature poses challenges for metal and ligand reuse and recovery, generating undesired waste and increasing their environmental footprint.^[2] Single-atom heterogeneous catalysts (SACs) attract substantial interest for bridging the gap between homogeneous and heterogeneous strategies.^[3a–c] Nonetheless, their applications have typically been limited to couplings of relatively simple partner molecules.^[3d] Advancing the design principles of SACs for more complex transformations requires knowledge of their structure and function in reactive environments, which is currently limited for surface-catalyzed organic reactions,^[4] due to the constraints of existing *in-situ* characterization approaches for tracking the state of metal centers under operating conditions.^[5] Most previous reports have concentrated on evaluating the stability of ill-defined supported metal nanoparticles, where insights from suitable techniques such as X-ray absorption spectroscopy (XAS) likely reflect an average state of distinct palladium species (e.g., nanoparticles, clusters, isolated atoms), or involve batch experiments with minimal control over the catalyst–reaction medium contact time.^[6]

Here, we develop droplet-based microfluidics platforms to facilitate *in-situ* XAS analysis, unlocking valuable insights into the structure and mechanisms of cross-coupling reactions over heterogeneous catalysts. Our focus is on exploring a palladium SAC based on exfoliated graphitic carbon nitride (Pd_{SA}@ECN, 2.23 wt % Pd content) whose synthesis and properties are well established, and which is known to exhibit selective and stable performance in Suzuki–Miyaura coupling.^[7] Besides the broad relevance of this reaction, another compelling reason for its selection is the availability of *in-situ* data for homogeneously catalyzed systems,^[6c] which facilitates relevant comparisons. High-angle annual dark field scanning transmission electron microscopy (HAADF-STEM) imaging (Figure S1, Figure S2) and Fourier transform extended X-ray absorption fine structure (FT-EXAFS) and X-ray absorption near edge structure (XANES) spectra (Figure S3, Figure S4a) confirm the isolated nature and oxidized character (Pd^{II}) of the palladium species in the as-synthesized Pd_{SA}@ECN. While previous density functional theory (DFT) simulations suggested a similar reaction path to classical homogeneous catalysis (Scheme 1),^[7] experimental verification of i) the adaptive coordination of palladium centers proposed to facilitate charge transfer and ii) the role of ligands and other reaction components, is lacking.

Droplet-based microfluidics offers a novel approach for studying heterogeneous catalysts. Our developed XAS plat-

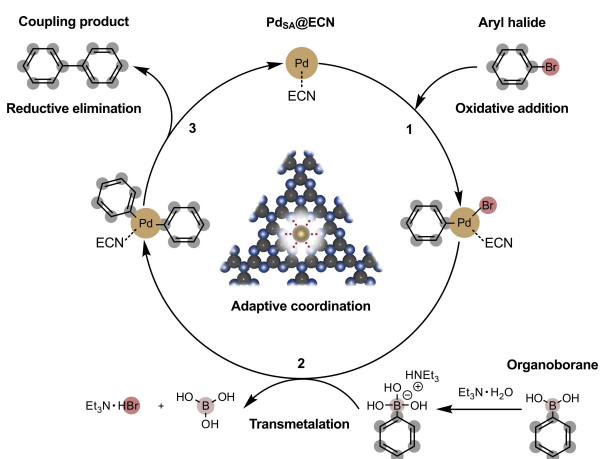
[*] T. Moragues, Dr. G. Giannakakis, Prof. A. J. de Mello, Prof. J. Pérez-Ramírez, Dr. S. Mitchell
 Institute of Chemical and Bioengineering
 Department of Chemistry and Applied Biosciences
 ETH Zürich
 Vladimir-Prelog-Weg 1, Zürich 8093, Switzerland
 E-mail: andrew.demello@chem.ethz.ch
 jpr@chem.ethz.ch
 msharon@chem.ethz.ch

A. Ruiz-Ferrando
 Institute of Chemical Research of Catalonia (ICIQ-CERCA)
 Av. Països Catalans 16, Tarragona 43007, Spain

A. Ruiz-Ferrando
 University of Rovira i Virgili
 Av. Catalunya 35, Tarragona 43002, Spain

Dr. C. N. Borca, Dr. T. Huthwelker, Dr. A. Bugaev
 Paul Scherrer Institute
 Forschungsstrasse 111, Villigen 5232, Switzerland

© 2024 The Authors. Angewandte Chemie International Edition published by Wiley-VCH GmbH. This is an open access article under the terms of the Creative Commons Attribution License, which permits use, distribution and reproduction in any medium, provided the original work is properly cited.



Scheme 1. Previously proposed Suzuki–Miyaura coupling mechanism over a $\text{Pd}_{\text{SA}}@ECN$ catalyst, resembling the classical cycle over metal complexes.^[7] The adaptive coordination of the catalyst during reaction lacks experimental verification.

forms generate nanoliter reaction vessels,^[8a] containing catalyst suspensions and required reagents at user-defined concentrations. Despite challenges related to solid dispensing,^[8b] this approach permits precise control over the contact time between the catalyst and reagent streams making it particularly suited for investigating chemical reactions at low conversions in the kinetic

regime. Importantly, the constant renewal of droplets under X-ray illumination also avoids potential radiation-induced damage to the studied materials during XAS measurements.^[8c] The platform designs require optimization for operation at different energy ranges. Specifically, the L_3 -edge platform incorporates a microchannel network forming coils of exponentially longer residence times around a central measurement channel (Figure 1a, Figure S5).^[9] To maximize fluorescence count rates, the device is mounted on an X-ray transparent Si_3N_4 window (Figure 1b).^[10] In contrast, when working at the K -edge, a thin glass slide is used, with minimal loss of signal due to the high energy of the emitted photons. Considering the lower sensitivity of the K -compared to the L_3 -edge due to the lower absorption cross-section at higher energy, we modified the device geometry, integrating larger channels distributed linearly across the surface. This enables generation of larger droplets and analysis along entire channels length to maximize signal (Figure 1c, Figure S6). The K -edge platform allows simultaneous measurements in transmission and fluorescence XAS. In this study, we focus solely on fluorescence due to the low signal-to-noise ratio in transmission caused by the dilute palladium concentration in the reaction mixture. At this edge, a heating stage enables the study of reactions at temperatures up to 70°C (Figure 1d), which was not feasible within the current study at the L_3 -edge due to beamline constraints.

For *in-situ* catalytic measurements, we adopt similar conditions to those previously optimized for $\text{Pd}_{\text{SA}}@ECN$,^[7] with

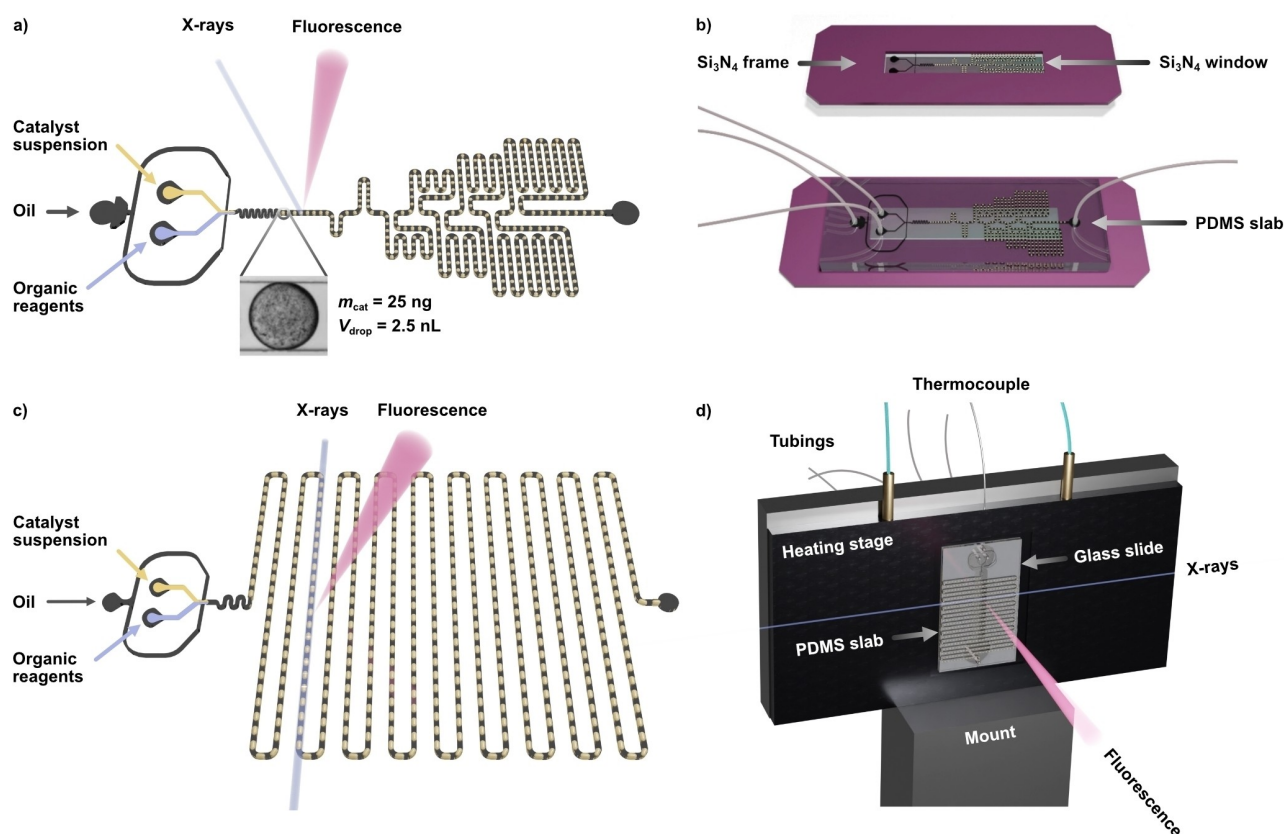


Figure 1. a) Scheme of the channel pattern and operation principle and b) bottom and top-view images of the L_3 -edge microfluidic device. c) Scheme of the channel pattern and operation principle and d) front view of the K -edge microfluidic device.

minor adjustments such as substituting K_2CO_3 with an organic base (triethylamine, TEA) to address solubility issues, and using 1,4-dioxane instead of dimethoxyethane to ensure compatibility with device materials. The catalyst is suspended in distilled water, while reagents are dissolved in a monophasic water/ethanol/1,4-dioxane solvent mixture, optimal for microfluidic measurements as it permits stable droplet generation (Movie S1). Using this approach, we designed a series of experiments to isolate the effects of the reaction mixture and different reaction components on the geometric and electronic structure of palladium centers in $Pd_{SA}@ECN$. Due to challenges associated with separating the catalytic particles after the microfluidic experiments, online monitoring of the performance of $Pd_{SA}@ECN$ to link with the XAS observations was not feasible. Importantly, evaluation of the catalyst in batch tests under analogous conditions verified the reaction occurrence at

room temperature, albeit at a slower rate than at $70^\circ C$ (turnover frequency, *TOF*, of 0.04 versus 1.91 h^{-1} , Table S3). Moreover, blank tests in the absence of $Pd_{SA}@ECN$ confirmed the absence of product formation.

In this frame, we successfully captured both the electronic and coordination environment of palladium centers in $Pd_{SA}@ECN$ through *in-situ* L_3 - and K -edge XAS measurements during Suzuki–Miyaura coupling using droplet-based microfluidics (Table S2). *Ex-situ* analysis of catalysts drop-cast from reaction mixtures highlighted a decreased sensitivity to structural changes between experimental conditions (Figure 2a,b) and the need for *in-situ* investigations. In the case of homogeneous catalysts, the classical mechanism of Suzuki–Miyaura coupling involves a Pd^0/Pd^{II} cycle during which the oxidative addition of the aryl halide is rate limiting, implying that a high population of metal centers is observed in the Pd^0 state at any

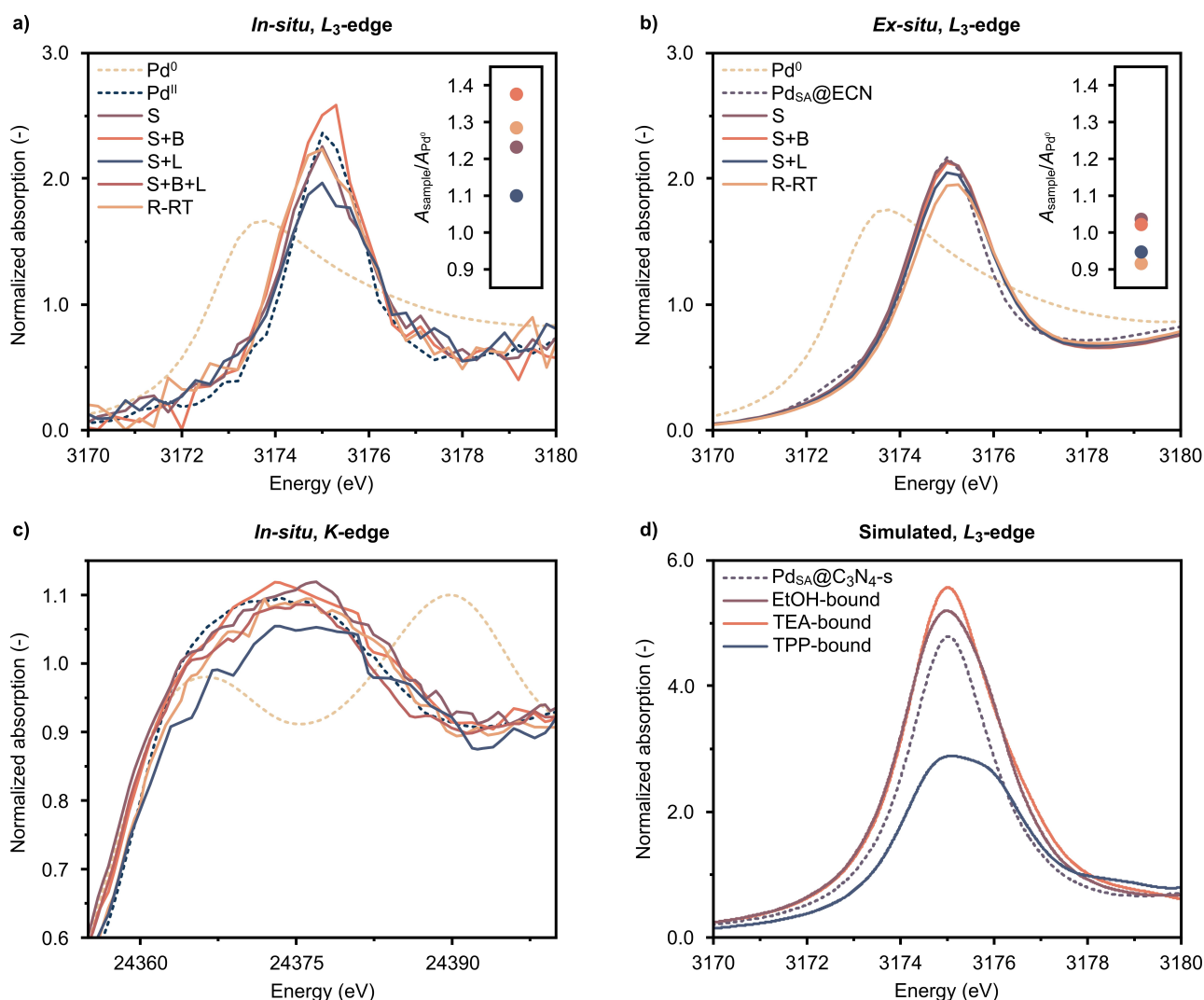


Figure 2. a) *In-situ* and b) *ex-situ* Pd L_3 -edge, and c) *in-situ* Pd K -edge XANES spectra of $Pd_{SA}@ECN$ acquired at room temperature during Suzuki–Miyaura coupling of phenylboronic acid and bromobenzene (R-RT) or in the presence of individual reaction components (S-solvent; B-base; L-ligand; and combinations thereof), compared to Pd^0 and Pd^{II} reference compounds. Insets in a) and b) display normalized L_3 -edge white line areas (Figure S7). d) Simulated Pd L_3 -edge XANES spectra of $Pd_{SA}@C_3N_4$ -s in the presence or absence of adsorbed ethanol (EtOH) representing the solvent, triethylamine (TEA) base, or triphenylphosphine (TPP) ligand. The legend in a) applies to c). Full reaction conditions are detailed in Table S2.

point during the reaction. The activation of the Pd^{II} pre-catalyst species into the active Pd⁰ form has been reported to occur on a similar timescale to the residence time achieved within our microfluidic platforms (<1 min), with the concurrent observation of a palladium–halide bond.^[6d] Comparison of the XANES spectra of Pd_{SA}@ECN under reaction conditions at room temperature and 70 °C (Figure 2a,c, Figure 3a) to relevant reference compounds reveals that palladium species exhibit a distinct electronic state close to Pd^{II} under both conditions. Considering the short time scale of the microfluidic experiments, we conducted *quasi in-situ* measurements of batch tests under analogous conditions at higher conversions (up to 70 %), confirming the absence of changes in the K-edge XANES spectra at 70 °C (*in-situ*, Figure 3a, *quasi in-situ*, Figure 3b). No Pd⁰ contribution was obtained by linear combination fitting under any conditions (Table S5). These results suggest mechanistic differences from homogeneous systems, particularly with respect to the predominant electronic state of palladium. This agrees with the previously proposed adaptation of the coordination structure to the charge on the metal center, in which the transmetalation step becomes rate limiting, and results in the observation of the Pd^{II} state.^[7] This difference in rate-limiting step is also corroborated by the lack of a noticeable Pd–Br bond signature in the *in-situ* FT-EXAFS spectra (inset Figure 3a), and supported by fits of the *quasi in-situ* measurements after 5 min of reaction at 70 °C (Figure S4b). It should be noted that this Pd–halide structure (proven to be stable under mild conditions)^[6d] is not expected to revert to its original state upon cooling to room temperature during the *quasi in-situ* measurements.

To unravel the roles of the ligand (L) and base (B), we decoupled their interactions with the metal center by acquiring *in-situ* XANES of the catalyst at the L₃-edge (Figure 2a,c) under controlled environments. This analysis reveals noticeable variations in the white line intensity of the L₃-edge, with the S+L combination displaying the lowest values compared to the

catalyst exposed only to the solvent (S). Such a drop may indicate partial reduction of palladium, but it most likely results from differences in the coordination environment. A similar coordination-induced variation is exemplified by the spread of white line intensities displayed by distinct Pd^{II} halides (Figure S8). The stability of the catalyst to leaching is confirmed by the retention of the metal in the Pd^{II} state. In the event of palladium species leaching into the reaction medium, solvated Pd⁰ species similar to the homogeneous Pd(TPP)₄ metal complex would be expected due to the presence of triphenylphosphine (TPP) ligands. However, the formation of such species is not observed (Figure S9). Instead, we propose that the drop in white line intensity stems from the electron-donating capability of TPP, which can coordinate to palladium. Conversely, the addition of TEA, a coordinating base, to a suspension of catalyst in solvent (S+B) leads to higher white line intensities at the L₃-edge. Similar observations are conveyed by measurements at the K-edge (Figure 2c), but with less sensitivity. Interestingly, when adding the base and ligand together, an intermediate line is obtained, suggesting that a competition for the coordination on the metal center occurs between the two species.

To gain further insight into the experimental trends, we conducted DFT simulations to identify the most energetically favorable configurations of palladium centers stabilized on a graphitic carbon nitride support (C₃N₄), representing the structure of ECN, in the presence of distinct reaction components. Palladium atoms can occupy different positions within the layered structure of graphitic carbon nitride (Table S6), but only those located at the surface (denoted Pd_{SA}@C₃N₄-s) are expected to participate in the reaction. Calculation of the L₃-edge spectra based on the structures of TPP, TEA, or EtOH bound to Pd_{SA}@C₃N₄-s using the full potential finite difference method of the FDMNES program evidenced a good agreement with the experimentally observed trends (Figure 2d).^[12] The simulations indicate that the adsorp-

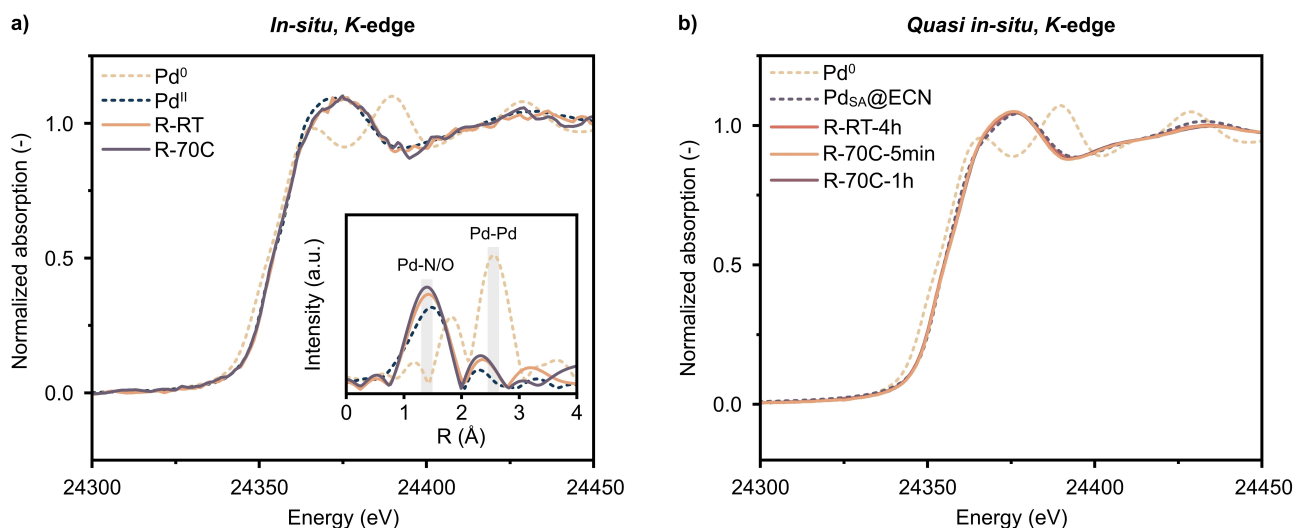


Figure 3. a) *In-situ* Pd K-edge XANES spectra of Pd_{SA}@ECN under full reaction conditions, acquired at room temperature (R-RT) or at 70 °C (R-70C). Inset displays the corresponding FT-EXAFS spectra. b) *Quasi in-situ* K-edge XANES spectra of Pd_{SA}@ECN under full reaction conditions, acquired at room temperature (R-RT-4h) and at 70 °C (R-70C-5min, R-70C-1h). Corresponding conversions are provided in Table S3.

tion of TPP over palladium in $\text{Pd}_{\text{SA}}@\text{C}_3\text{N}_4\text{-s}$ is favorable ($E_{\text{bind}} = -2.17$ eV, Table S7), and influences the local structure of the palladium atom at the surface of carbon nitride (Figure 4). Indeed, strong binding with the ligand keeps palladium in the surface layer of this two-dimensional host, while its resting state in the absence of TPP would be located in the subsurface, where it is at least 0.6 eV more favorable (Table S6). Inversely, the favored coordination of TEA to $\text{Pd}_{\text{SA}}@\text{C}_3\text{N}_4\text{-s}$ ($E_{\text{bind}} = -1.11$ eV) withdraws electrons from the metal and causes the intensity increase of the L_3 -edge line. We believe that although TPP adsorbs more favorably, the large excess of TEA (10-times excess, see Table S1) compensates for it kinetically, explaining the intermediate line observed in the K -edge spectra in the presence of both ligand and base (Figure 2c). Finally, the impact of the ligand and the base on the electronic state of the palladium atom are evidenced by the differences in the Bader charges and the projected density of states (PDOS) charge between the 3 cases, i) bare $\text{Pd}_{\text{SA}}@\text{C}_3\text{N}_4\text{-s}$, ii) TPP-bound, and iii) TEA-bound (Figure S10, Table S7). While the Bader charges do not present significant changes, indicating that the formal oxidation states are very close, the d -band center for TPP-bound $\text{Pd}_{\text{SA}}@\text{C}_3\text{N}_4\text{-s}$ located at lower energies than TEA-bound $\text{Pd}_{\text{SA}}@\text{C}_3\text{N}_4\text{-s}$ confirms the stabilizing effect of the ligand over the base. That said, it is worth noting that the comparison between computed oxidation states and formal ones as described in the $\text{Pd}^0/\text{Pd}^{\text{II}}$ cycle is difficult, as individual atomic charges in multi-electronic compounds are not quantum mechanical observables.^[13]

In conclusion, we have provided new insights into the mechanism of Suzuki–Miyaura coupling over a palladium single-atom heterogeneous catalyst, enabled by the development of versatile *in-situ* droplet-based XAS platforms. Our findings corroborate a fully heterogeneous, surface-catalyzed pathway. The electronic structure of the palladium remained largely constant, the metal centers maintaining a state close to Pd^{II}

during the reaction, consistent with the expected adaptive coordination to the carbon nitride host. Furthermore, we evidenced the previously unexplored stabilizing role of phosphine ligands and triethylamine base, as corroborated by DFT. This innovative approach points to distinct design criteria for homogeneous and heterogeneous catalysts, advancing our understanding of surface catalyzed reactions in organic syntheses. These insights are crucial for unlocking the potential of SACs in such transformations. The provided fabrication blueprints enhance accessibility to *in-situ* XAS studies, with potential applications to other liquid-phase reactions. The current platforms are particularly suited for studying transformations with fast kinetics, but the design can be readily modified to increase the range of measurable residence times. Additionally, the development of complementary approaches (e.g., infrared, electron paramagnetic resonance, nuclear magnetic resonance spectroscopy) will be valuable in overcoming existing constraints posed by *in-situ* XAS studies.

Supporting Information

Supporting Information is available from the Wiley Online Library or from the authors. The authors have cited additional references within the Supporting Information (Ref. [14–18]).

Acknowledgements

This publication was created as part of NCCR Catalysis (grant number 180544), a National Centre of Competence in Research funded by the Swiss National Science Foundation. We thank Prerit Mathur and Joel Jenni for fabricating the mount used for hard X-rays experiments, Adam Clark for

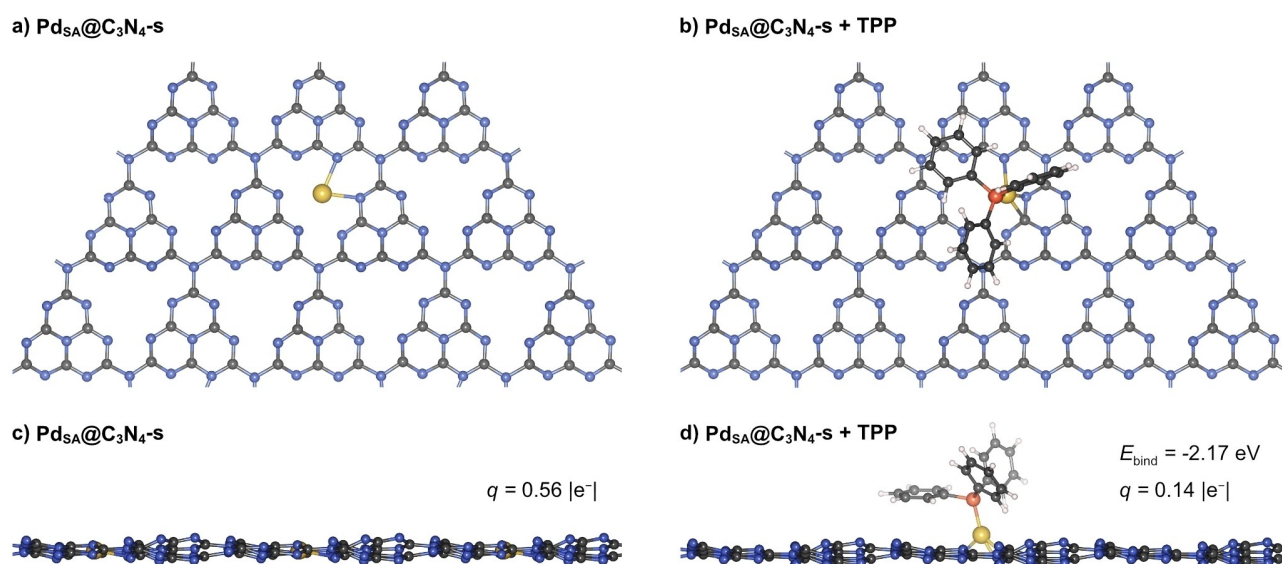


Figure 4. Molecular models of bare a,b) $\text{Pd}_{\text{SA}}@\text{C}_3\text{N}_4\text{-s}$ catalyst and c,d) following adsorption of the TPP ligand $\text{Pd}_{\text{SA}}@\text{C}_3\text{N}_4\text{-s}$ in top and side views, respectively. The calculated Bader charge (q) and, in the TPP-bound system, binding energy (E_{bind}) are indicated. Atom color codes: blue-nitrogen; dark grey-carbon; yellow-palladium; orange-phosphorus; white-hydrogen.

valuable help during K-edge measurements, and Chao Song for assistance with surface treatment of the microfluidic devices. We acknowledge the Paul Scherrer Institute, Villigen, Switzerland, for provision of beamtime at the PHOENIX and Super XAS beamlines of the Swiss Light Source (SLS) and the Scientific Center for Optical and Electron Microscopy at ETH Zürich (ScopeM) for access to their facilities. Open Access funding provided by Eidgenössische Technische Hochschule Zürich.

Conflict of Interest

The authors declare no conflict of interest.

Data Availability Statement

The data that support the findings of this study are openly available in Zenodo at <https://doi.org/10.5281/zenodo.8399256>. All DFT simulated structures are available on the ioChem-BD database at <https://iochem-bd.iciq.es/browse/review-collection/100/65349/cb5fd957f9feef7152f224b>.

Keywords: Droplet-based microfluidics · *in-situ* X-ray absorption spectroscopy · single-atom heterogeneous catalyst · cross-coupling mechanisms · electronic structure

- [1] a) R. Dorel, C. P. Grugel, A. M. Haydl, *Angew. Chem. Int. Ed.* **2019**, *58*, 17118; b) V. M. Chernyshev, V. P. Ananikov, *ACS Catal.* **2022**, *12*, 1180.
- [2] D. Faust Akl, D. Poier, S. C. D'Angelo, T. P. Araújo, V. Tulus, O. V. Safonova, S. Mitchell, R. Marti, G. Guillén-Gosálbez, J. Pérez-Ramírez, *Green Chem.* **2022**, *24*, 6879.
- [3] a) S. K. Kaiser, Z. Chen, D. Faust Akl, S. Mitchell, J. Pérez-Ramírez, *Chem. Rev.* **2020**, *120*, 11703; b) X. Cui, W. Li, P. Ryabchuk, K. Junge, M. Beller, *Nat. Catal.* **2018**, *1*, 385; c) G. Giannakakis, S. Mitchell, J. Pérez-Ramírez, *Trends Chem.* **2022**, *4*, 264; d) E. Vorobyeva, V. C. Gerken, S. Mitchell, A. Sabadell-Rendón, R. Hauert, S. Xi, A. Borgna, D. Klose, S. M. Collins, P. A. Midgley, D. M. Kepaptsoglou, Q. M. Ramasse, A. Ruiz-Ferrando, E. Fako, M. A. Ortuño, N. López, E. M. Carreira, J. Pérez-Ramírez, *ACS Catal.* **2020**, *10*, 11069.
- [4] a) G. Ding, L. Hao, H. Xu, L. Wang, J. Chen, T. Li, X. Tu, Q. Zhang, *Commun. Chem.* **2020**, *3*, 1; b) S. Ji, X. Lu, M. Zhang, L. Leng, H. Liu, K. Yin, C. Xu, C. He, J. H. Horton, J. Zhang, Z. Li, *Chem. Eng. J.* **2023**, *452*, 139205; c) J. Liu, Z. Chen, C. Liu, B. Zhang, Y. Du, C.-F. Liu, L. Ma, S. Xi, R. Li, X. Zhao, J. Song, X. Z. Sui, W. Yu, L. Miao, J. Jiang, M. J. Koh, K. P. Loh, *J. Mater. Chem. A* **2021**, *9*, 11427; d) I. Romero-Muñiz, A. Mavrandonakis, P. Albacete, A. Vega, V. Briois, F. Zamora, A. E. Platero-Prats, *Angew. Chem. Int. Ed.* **2020**, *59*, 13013.
- [5] a) X. Li, X. Yang, J. Zhang, Y. Huang, B. Liu, *ACS Catal.* **2019**, *9*, 2521; b) I. Beckers, A. Bugaev, D. De Vos, *Chem. Sci.* **2023**, *14*, 1176; c) G. A. Somorjai, S. K. Beaumont, S. Alayoglu, *Angew. Chem. Int. Ed.* **2011**, *50*, 10116.
- [6] a) P. Zimmermann, S. Peredkov, P. M. Abdala, S. DeBeer, M. Tromp, C. Müller, J. A. van Bokhoven, *Coord. Chem. Rev.* **2020**, *423*, 213466; b) L. Negahdar, C. M. A. Parlett, M. A. Isaacs, A. M. Beale, K. Wilson, A. F. Lee, *Catal. Sci. Technol.* **2020**, *10*, 5362; c) P. J. Ellis, I. J. S. Fairlamb, S. F. J. Hackett, K. Wilson, A. F. Lee, *Angew. Chem. Int. Ed.* **2010**, *49*, 1820; d) G. Giulera, M. A. Newton, C. Polli, S. Pascarelli, M. Guinó, K. K. Hii, *Chem. Commun.* **2006**, *41*, 4306.
- [7] Z. Chen, E. Vorobyeva, S. Mitchell, E. Fako, M. A. Ortuño, N. López, S. M. Collins, P. A. Midgley, S. Richard, G. Vilé, J. Pérez-Ramírez, *Nat. Nanotechnol.* **2018**, *13*, 702.
- [8] a) T. Moragues, D. Arguijo, T. Beneyton, C. Modavi, K. Simutis, A. R. Abate, J.-C. Baret, A. J. deMello, D. Densmore, A. D. Griffiths, *Nat. Rev. Methods Primers* **2023**, *3*, 1; b) T. Moragues, S. Mitchell, D. Faust Akl, J. Pérez-Ramírez, A. deMello, *Small Structures* **2023**, *4*, 2200284; c) W. Bras, M. A. Newton, D. A. A. Myles, R. Felici, *Nat. Rev. Methods Primers* **2022**, *2*, 1.
- [9] a) D. Hess, T. Yang, S. Stavrakis, *Anal. Bioanal. Chem.* **2020**, *412*, 3265; b) J. Probst, C. N. Borca, M. A. Newton, J. van Bokhoven, T. Huthwelker, S. Stavrakis, A. deMello, *ACS Meas. Sci. Au* **2021**, *1*, 27.
- [10] B. L. Henke, E. M. Gullikson, J. C. Davis, *At. Data Nucl. Data Tables* **1993**, *54*, 181.
- [11] B. Sun, L. Ning, H. C. Zeng, *J. Am. Chem. Soc.* **2020**, *142*, 13823.
- [12] a) A. A. Guda, S. A. Guda, M. A. Soldatov, K. A. Lomachenko, A. L. Bugaev, C. Lamberti, W. Gawelda, C. Bressler, G. Smolentsev, A. V. Soldatov, Y. Joly, *J. Phys. Conf. Ser.* **2016**, *712*, 012004; b) S. A. Guda, A. A. Guda, M. A. Soldatov, K. A. Lomachenko, A. L. Bugaev, C. Lamberti, W. Gawelda, C. Bressler, G. Smolentsev, A. V. Soldatov, Y. Joly, *J. Chem. Theory Comput.* **2015**, *11*, 4512.
- [13] A. Walsh, A. A. Sokol, J. Buckeridge, D. O. Scanlon, C. R. A. Catlow, *Nat. Mater.* **2018**, *17*, 958.
- [14] K. Rossi, A. Ruiz-Ferrando, D. Faust Akl, V. Gimenez Abalos, J. Heras-Domingo, R. Graux, X. Hai, J. Lu, D. Garcia-Gasulla, N. López, J. Pérez-Ramírez, S. Mitchell, *Adv. Mater.* **2024**, *36*, 2307991; <https://huggingface.co/spaces/nccr-catalysis/atom-detection>.
- [15] a) Z. Chen, S. Mitchell, F. Krumeich, R. Hauert, S. Yakunin, M. V. Kovalenko, J. Pérez-Ramírez, *ACS Sustainable Chem. Eng.* **2019**, *7*, 5223; b) K. Shimizu, Y. Kamiya, K. Osaki, H. Yoshida, A. Satsuma, *Catal. Sci. Technol.* **2012**, *2*, 767; c) A. V. Dobrovolskaya, S. V. Chapek, O. A. Usoltsev, E. Naranov, D. N. Gorbunov, A. L. Trigub, A. L. Maximov, A. V. Soldatov, A. L. Bugaev, *J. Phys. Chem. C* **2023**, *127*, 20727.
- [16] a) A. H. Clark, J. Imbao, R. Frahm, M. Nachttegaal, *J. Synchrotron Radiat.* **2020**, *27*, 551; b) M. Newville, *J. Synchrotron Radiat.* **2001**, *8*, 322.
- [17] a) A. Martini, S. A. Guda, A. A. Guda, G. Smolentsev, A. Algasov, O. Usoltsev, M. A. Soldatov, A. Bugaev, Yu. Rusalev, C. Lamberti, A. V. Soldatov, *Comput. Phys. Commun.* **2020**, *250*, 107064; b) G. Kresse, J. Furthmüller, *Comput. Mater. Sci.* **1996**, *6*, 15; c) G. Kresse, *J. Furthmüller, Phys. Rev. B* **1996**, *54*, 11169; d) J. P. Perdew, K. Burke, M. Ernzerhof, *Phys. Rev. Lett.* **1996**, *77*, 3865.
- [18] a) S. Grimme, S. Ehrlich, L. Goerigk, *J. Comput. Chem.* **2011**, *32*, 1456; b) N. Almora-Barrios, G. Carchini, P. Błoński, N. López, *J. Chem. Theory Comput.* **2014**, *10*, 5002; c) G. Kresse, D. Joubert, *Phys. Rev. B* **1999**, *59*, 1758; d) P. E. Blöchl, *Phys. Rev. B* **1994**, *50*, 17953; e) M. Álvarez-Moreno, C. de Graaf, N. López, F. Maseras, J. M. Poblet, C. Bo, *J. Chem. Inf. Model.* **2015**, *55*, 95; f) A. Ruiz-Ferrando, *ioChem-BD* **2023**. <https://iochem-bd.iciq.es/browse/review-collection/100/65349/cb5fd957f9feef7152f224b>.

Manuscript received: January 16, 2024

Accepted manuscript online: March 12, 2024

Version of record online: April 2, 2024